Supplemental Information

Supplemental Figure Legends:

Fig. S1. Identification of LRRK2-interacting phosphoproteins and kinase substrates, Related to Figure 1. (**A**), cytoscape network analysis of LRRK2-interacting phosphoproteins reveals four major functional groups as shown. Each group consists of nodes (molecular functions) connected to indicate functional relationships between nodes, and each group is headed by its statistically most represented function. Ungrouped nodes are white and not connected to other nodes. (**B**), scheme for screening LRRK2-interacting phosphoproteins in LRRK2 kinase assays. (**C**), autoradiograms, coomassie stained polyacrylamide gels and quantitation of LRRK2 substrate ^{32}P incorporation. Phosphorylation was decreased via D1994A (kinase-dead) and increased by G2019S or I2020T LRRK2 for some substrates as indicated (individual ANOVAs followed by Bonferroni's post-test, $*$ $p < 0.05$, $**$ $p < 0.01$, $***$ $p < 0.001$, $n = 3$). Data are mean ± SEM.

Fig. S2. LRRK2 substrate phosphorylation sites and role in pathogenic LRRK2 toxicity, Related to Figure 2. Phospho-site spectra for (**A**) s11 and (**B**) s15 threonine phosphorylation sites (pT) identified following incubation with WT LRRK2 are shown. No phosphorylation sites were detected following D1994A LRRK2 incubation with either substrate (not shown). Sequence coverage by tandem mass spectrometry is indicated by underlined text and phosphorylation sites are indicated by arrows. (**C**), A triple mutation of threonines 28, 46 and 54 (TM s11) eliminates LRRK2 phosphorylation.

Effect of TM s11 expression on G2019S LRRK2-induced toxicity (individual ANOVAs, Bonferroni's post-test ∗∗∗ $p<0.001$, n =3). Scale bar, 25 µM. Data are mean ± SEM. (**D**), effects of T136A(TA) s15 on I2020T or R1441C LRRK2 toxicity assessed in rat cortical neurons. Arrows indicate neurons lacking neurites, a subset of which are TUNEL-positive (see inset magnifications) as indicated. T136A s15 protects against I2020T LRRK2 neurite toxicity and cell death (individual ANOVAs, Bonferroni post-test, ∗ $p<0.05$, ∗∗ $p<0.01$, ∗∗∗ $p<0.001$, n =3). Data are mean ± SEM.

Fig. S3. Characterization of ES cell-derived human cortical and midbrain dopamine neurons and Phospho-T136 antibody validation, Related to Figure 3. (**A**), Human dopamine neurons are immunopositive for tyrosine hydroxylase (TH), the midbrain marker FOXA2 and neuronal marker TUJ1 at 32 d of differentiation. (**B**), Human cortical neurons are immunopositive for MAP2, cortical neuron layer markers as indicated and synaptophysin at 60 d of differentiation. Scale bar, 25 µM except synaptophysin, 5 µM. (**C**), T136 phospho-s15 is significantly increased by G2019S LRRK2 expression in human cortical neurons (ANOVA followed by Bonferroni's post-test, ∗ $p<0.05$, n =3). (**D**), ELISA showing T136 Phospho-s15 primary antibody dilution curve for binding to T136 Phospho-s15 or s15 oligopeptide. (**E**), Dot blot showing binding of T136 Phospho-s15 antibody to T136 Phospho-s15 or s15 oligopeptide. (**F**), *In vitro* LRRK2 kinase assay and immunoblot showing specific antibody binding to T136 Phospho-s15 following LRRK2-mediated s15 phosphorylation. (**G**), s15 knock-down (yellow arrowheads) partially rescues G2019S LRRK2 toxicity (neurite shortening and cell death) in human cortical neurons (individual ANOVAs, Bonferroni's post-test, ∗

p<0.05, ∗∗ p<0.01, ∗∗∗ p<0.001). Scale bar, 25 μM. LRRK2 levels are not affected by s15 knock-down. (**H**), LRRK2 toxicity in rat cortical neurons mediated by low (125 pM plasmid) or high (0.4 nM plasmid) levels of LRRK2. Scale bar, 20 μM. Quantitation of the data revealed that increasing wild-type LRRK2 expression increases neuronal injury and cell death (ANOVA, Bonferroni's post-test, ∗∗ p<0.01, ∗∗∗ p<0.001, n =3). The vast majority of GFP-positive neurons (~90%) co-labeled for LRRK2 when co-transfected (not shown). (**I**), P-s15 levels in rat neuron ribosomal fractions following LRRK2 overexpression (∗ p<0.05, ∗∗ p<0.01, n =3). Data are mean ± SEM.

Fig. S4. Block of s15 phosphorylation block by LRRK2 kinase inhibitors, Related to Figure 4. (**A**), the LRRK2 kinase inhibitor LRRK2-IN-1 inhibited autophosphorylation of recombinant LRRK2 and LRRK2-mediated s15 phosphorylation. IC_{50} values derived from the dose-response curve are indicated. n=3. (**B**), the LRRK2 kinase inhibitor CZC-25146 blocked recombinant LRRK2-mediated s15 phosphorylation and inhibited V5-s15 phosphorylation via G2019S LRRK2 in co-transfected HEK293 cells (ANOVA, Bonferroni's post-test, ∗ p<0.05, n =3). (**C**), colocalization controls for LRRK2 and s15 interaction show absence of spectral cross-talk between red and green channels for confocal microscopy conditions used. Overexpressed G2019S LRRK2 and s15 exhibit perinuclear colocalization. Scale bars, 10 μM. Scale bars, 10 μM. (**D**), immunoprecipitated V5-s15 (N-terminal tag) co-immunoprecipitated full-length FLAG tagged LRRK2 and its WD40 domain. Data are representative of three independent experiments. (**E**), Co-immunoprecipitation of endogenous LRRK2 and s15 from human HEK293 cells. Results are representative of three independent experiments. (**F**) LRRK2

expression in post-mortem brain whole lysates. (**G**), perinuclear colocalization of endogenous s15 and dLRRK in Drosophila S2 cells. Scale bars, 10 µM. Data are mean ± SEM.

Fig. S5. s15 expression and dopamine neuron viability in transgenic *Drosophila*, Related to Figure 5. (**A**), Immunoblot confirmation of *UAS-s15* and *UAS-T136A s15* expression via *da-Gal4* in male fly heads. Similar expression levels were observed in females. (**B**)**,** no effect of s15 or T136A s15 co-expression on G2019S LRRK2 expression via *Ddc-Gal4*. (**C**), no significant effect of G2019S LRRK2, s15 or T136A s15 expression via *Ddc-Gal4* on dopamine neurons in the major posterior clusters (PPM1/2, PPM3, PPL1, PPL2) or anterior PAL cluster in 3 week-old flies (individual ANOVAs for each dopamine neuron cluster visualized by TH immunostaining). Scale bar, 60 µM. (**D**), negative geotaxis in 2-week-old LRRK2 and s15 transgenic flies. (**E**), no significant effect of s15 or T136A s15 expression alone on negative geotaxis ability or (**F**) dopamine neurons numbers. Data are mean ± SEM.

Fig. S6. Bicistronic reporter expression in human cortical neurons and neuroblastoma cells, Related to Figure 6. (**A**), reporter mRNA levels at the maximum amount of LRRK2 and s15 plasmid transfected in SH-SY5Y cells in Figs. 6B and C. There were no significant effects of LRRK2 or s15 variant expression on reporter mRNA levels (individual ANOVAs, n =3). (**B**), s15 knock-down via shRNA in human SH-SY5Y cells attenuates G2019S LRRK2-induced bicistronic reporter expression whereas expressing non-targeting shRNA to mouse s15 did not (individual ANOVAs, Bonferroni's

post-test, ∗ p<0.05, ∗∗ p<0.01, ∗∗∗ p<0.001). (**C**), no effect of dicer silencing and no modulation of G2019S LRRK2 effect by hAgo2 overexpression on cap-dependent and cap-independent reporter translation in SH-SY5Y cells. Scr is scrambled control siRNA. (**D**), 4E-BP1 overexpression did not block G2019S LRRK2-induced cap-dependent (c.d.) or cap-independent (c.i.) translation. (**E**), 4E-BP1 phosphorylation was unaffected by G2019S LRRK2 expression in SH-SY5Y cells. (**F**), phospho-4EBP1 (Thr 37/46) is not increased in G2019S transgenic fly heads. (**G**), reduced eIF4E expression in Drosophila by two independent mutant alleles, $4E^{07235}$ and $4E^{67Af}$. (**H**), locomotor deficits seen in aged (5 weeks) G2019S transgenic flies are not significantly affected by reduced 4E expression. (**I**), loss of dopamine neurons observed in aged G2019S transgenic flies is not affected by reduced 4E expression. (**J**), neuronal toxicity and cell death were significantly higher in reporter-positive neurons compared to surrounding reporter-negative neurons (MAP2 positive). Individual two-way ANOVAs, ∗∗∗ p < 0.001, ∗∗∗∗ p < 0.0001, n = 4. Scale bar, 25 μM. Data are mean ± SEM.

Fig S7. Ribosomal run-off following harringtonine treatment is unaffected by G2019S LRRK2, Related to Figure 7. (**A**), schematic of harringtonine and cycloheximide treatment. (**B**), polysome profiles generated at indicated time points following harringtonine treatment of SH-SY5Y cells demonstrate progressive ribosomal run-off. (**C**), no significant difference of ribosomal run-off, quantified as polysome area under curve (AUC) at each time point between cells transfected with vector, G2019S/D1994A LRRK2 or G2019S LRRK2 (two-way ANOVA, Bonferroni's post-test, n =3) (**D**), no significant difference in ribosomal run-off, measured by increase in 35S-

met/cys incorporation following harringtonine treatment (two-way ANOVA, Bonferroni's post-test, n =3). (**E**), anisomycin treatment had no effect on LRRK2 expression (Student's t-test, ns, n=3). (**F**), anisomycin treatment had no effect on P-s15 levels in fly head whole lysates (Lys) or ribosomal fractions (Ribo). Genotypes for (**E**) and (**F**) are *Da-Gal4/+; +/+* (Control) and *Da-Gal4/+; G2019S-LRRK2/+* (G2019S). (**G**), Anisomycin treatment reduced the elevated protein synthesis in G2019S transgenic flies (ANOVA, Bonferroni's post-test, * $p<0.05$, n =3). Data are mean ± SEM.

Supplemental Tables

Table S1. LRRK2-interacting proteins, Related to Figure 1.

Supplied as an Excel format file

Table S2. Ribosomal protein purification and kinase screening results, Related to Figure 1.

Protein	Purified (Y/N)	LRRK2 Substrate (Y/N)
ribosomal protein L27 (RPL27)	Y	N
ribosomal protein S27a (RPS27a)	Y	N
ribosomal protein L19 (RPL19)	Y	N
ribosomal protein S15a (RPS15a)	N	N
ribosomal protein S13 (RPS13)	Y	Y
ribosomal protein L18 (RPL18)	Y	N
ribosomal protein L29 (RPL29)	Y	N
ribosomal protein L6 (RPL6)	N	N
ribosomal protein L13a (RPL13A)	N	N
ribosomal protein L15 (RPL15)	N	N
ribosomal protein S6 (RPS6)	Y	N
ribosomal protein L35a (RPL35A)	Y	N
ribosomal protein S11 (RPS11)	Y	Y
ribosomal protein L31 (RPL31)	Y	N
ribosomal protein L7 (RPL7)	N	N
ribosomal protein L27a (RPL27A)	N	N
ribosomal protein L21 (RPL21)	Y	Y
ribosomal protein L36a (RPL36A)	Y	Y
ribosomal protein L4 (RPL4)	Y	N
ribosomal protein L35 (RPL35)	Y	N
ribosomal protein L34 (RPL34)	Y	Y
ribosomal protein S10 (RPS10)	Y	N
ribosomal protein L41 (RPL41)	Y	N
ribosomal protein, large, P0 (RPLP0)	Y	N
ribosomal protein L7a (RPL7A)	Y	N
ribosomal protein L10 (RPL10)	Y	N
ribosomal protein S12 (RPS12)	Y	N
ribosomal protein L30 (RPL30)	Y	Y
ribosomal protein L39 (RPL39)	Y	Y
ribosomal protein L38 (RPL38)	Y	N
ribosomal protein L36 (RPL36)	Y	N
ribosomal protein S9 (RPS9)	Y	N
ribosomal protein SA (RPSA)	Y	N
ribosomal protein S17 (RPS17)	Y	N
ribosomal protein L28 (RPL28)	Y	N
ribosomal protein L37 (RPL37)	Y	N
ribosomal protein S24 (RPS24)	Y	N
ribosomal protein S29 (RPS29)	Y	N
ribosomal protein L37a (RPL37A)	N	N

ribosomal protein L18a (RPL18A)	Y	N
ribosomal protein S26 (RPS26)	Y	N
ribosomal protein L26 (RPL26)	Y	N
ribosomal protein S18 (RPS18)	Y	Y
ribosomal protein S21 (RPS21)	Y	N
ribosomal protein S25 (RPS25)	Y	N
ribosomal protein L17 (RPL17)	Y	Y
ribosomal protein S28 (RPS28)	Y	N
ribosomal protein L22 (RPL22)	Y	N
ribosomal protein L5 (RPL5)	Y	N
ribosomal protein L32 (RPL32)	Y	N
ribosomal protein S2 (RPS2)	Y	N
ribosomal protein S3 (RPS3)	Y	Y
ribosomal protein S3a (RPS3a)	Y	N
ribosomal protein S4 (RPS4)	Y	Y
ribosomal protein S8 (RPS8)	Y	N
ribosomal protein S5 (RPS5)	Y	N
ribosomal protein S7 (RPS7)	Y	N
ribosomal protein S14 (RPS14)	Y	N
ribosomal protein S15 (RPS15)	Y	Y
ribosomal protein S16 (RPS16)	Y	Y
ribosomal protein S19 (RPS19)	Y	N
ribosomal protein S20 (RPS20)	Y	N
ribosomal protein S23 (RPS23)	Y	Y
ribosomal protein S27 (RPS27)	Y	Y
ribosomal protein L3 (RPL3)	Y	N
ribosomal protein L9 (RPL9)	Y	N
ribosomal protein L10a (RPL10a)	Y	Y
ribosomal protein L11 (RPL11)	Y	N
ribosomal protein L12 (RPL12)	Y	N
ribosomal protein L13 (RPL13)	Y	Y
ribosomal protein L14 (RPL14)	Y	Y
ribosomal protein L23 (RPL23)	Y	N
ribosomal protein L23a (RPL23a)	Y	Y
ribosomal protein L24 (RPL24)	Y	N
ribosomal protein S30 (RPS30)	N	N
ribosomal protein L8 (RPL8)	N	N
ribosomal protein L2 (RPL2)	N	N
ribosomal protein L40 (RPL40)	N	N
Ribosomal protein, large, P1 (RPLP1)	N	N
Ribosomal protein, large, P2 (RPLP2)	N	N

Extended Experimental Procedures:

LRRK2 tandem affinity purification

A fusion protein consisting of full-length LRRK2 with a C-terminal Streptavidin binding peptide and calmodulin binding peptide tag (TAP LRRK2) was generated and transfected into HEK293 cells. 48 h following transfection, LRRK2 was purified from cells using the InterPlay mammalian tandem affinity purification (TAP) kit (Agilent) following the manufacturer's instructions. The TAP eluate was enriched for phosphoprotein using an immobilized metal affinity chromatography (IMAC) column. A fraction of the IMAC column eluate was subjected to an *in vitro* kinase assay with γ-^{32}P-ATP followed by SDS-PAGE and immunoblotting to confirm the purification of kinase-active LRRK2. Phosphorimaging revealed abundant incorporation of ^{32}P in a protein confirmed to be LRRK2 by immunoblotting, as well as ^{32}P incorporation in numerous co-purified proteins. The co-purification of numerous phospho-proteins by this method was also supported by phosphostaining a portion of the IMAC column eluate. All remaining eluate was resolved by SDS-PAGE. The gel was fixed and stained with coomassie brilliant blue revealing candidate LRRK2-interacting proteins with a wide range of molecular weights. The entire loaded lane was excised from the gel and divided into even sized gel fragments. All fragments were analyzed by mass spectrometry in order to identify candidate LRRK2 interacting proteins.

Cytoscape analysis of LRRK2 interacting proteins

LRRK2-interacting proteins were filtered to control for non-specific binding. Interacting proteins identified using TAP-tags for Botch and GADD45ß were subtracted from the

mass spectrometry data set for LRRK2. The remaining set of LRRK2-interacting proteins was analyzed using the ClueGo Cytoscape plugin with molecular function gene ontology annotation. Functional groups consist of nodes (molecular functions) connected to reflect functional relationships between nodes. Each functional group is annotated in colored type according to the statistically most enriched molecular function for that group. Ungrouped functional nodes are white and not connected to other nodes.

Generation of GST tagged candidate LRRK2 substrates

Entry clone cDNA for each of the LRRK2-interacting proteins identified by tandem affinity purification was sub-cloned into an N-terminal GST-tagged bacterial expression vector (pDEST 15, Invitrogen) via Gateway cloning and expressed in *E.coli* for affinity purification of GST tagged protein. Starter cultures for each expression clone were generated from single colonies grown overnight at 37°C, and a 200 µL aliquot was transferred to 3 ml LB broth and cultured at 37°C. Protein expression was induced using 0.15 mM IPTG once bacterial cultures had reached an O.D. of 0.6 a.u. At this time point, cultures were incubated at 30°C for 3 h, pelleted by centrifugation (3,000 x g for 10 minutes) and then lysed in chilled lysis buffer (BugBuster, 1 mg/ml lysozyme, protease inhibitor cocktail and benzonase nuclease) on ice for 30 minutes. Lysates were centrifuged at 16,000 x g for 20 minutes at 4°C, and the supernatant was incubated with glutathione sepharose beads (GE healthcare) resuspended in PBS overnight at 4°C with end-over-end rotation. The beads were separated from lysate by centrifugation and were washed three times in chilled PBS, followed by elution of bound

protein in elution buffer (50 mM HEPES (pH 8), 150 mM NaCl and 30 mM glutathione). Eluted proteins were stored in 15% glycerol at -20°C until use.

LRRK2 *in vitro* kinase assays

LRRK2 kinase assays were performed with purified recombinant GST-tagged LRRK2 (aa 970-2527) or its variants D1994A, G2019S and I2020T (Invitrogen) along with purified recombinant GST-tagged substrate candidate generated as described above. Proteins were incubated in a kinase assay buffer (20 mM HEPES pH 7.5, 5 mM EGTA, 20 mM β-glycerophosphate, 20 mM $MgCl_2$, 10 µM ATP and 0.5 µCi of γ-^{32}P-ATP at a combined volume of 30 µL. The reaction mixture was incubated at 30°C for 30 minutes, or as indicated. Reactions were quenched by the addition of SDS-sample loading buffer, heated to 70°C for 10 minutes and then loaded onto 8% polyacrylamide gels for SDS-PAGE. Following electrophoresis, gels were fixed (50% methanol, 10% acetic acid), stained in coomassie brilliant blue, heat-sealed in hybridization bags and exposed to a phosphorimaging screen overnight at room temperature for assessing radioactive ^{32}P incorporation. GST alone was not phosphorylated (not shown).

LRRK2 enzyme kinetics

LRRK2 kinase assays with recombinant LRRK2 and s15 were performed as described above, except reactions were incubated for 5 minutes at 30°C in order to measure initial enzyme velocity. To determine an appropriate time point for assessing initial enzyme velocity, time-course LRRK2 kinase assays were performed for a range of s15 concentrations to monitor the progress curve for LRRK2-catalyzed s15 phosphorylation.

After 5 minutes, product formation was detectable by autoradiography at all substrate concentrations tested, and estimation of product formation over time indicated that non-phosphorylated substrate concentration was still within 10% of its starting value. Additionally, measurements of s15 and LRRK2 stability under assay conditions indicated that both enzyme and substrate were stable over this time period, and hence this was a suitable period for measuring initial enzyme velocity. Estimates of Michaelis-Menten kinetic parameters K_m and V_{max} for s15 were derived from measurements of initial LRRK2 reaction velocity at varying s15 concentrations using non-linear regression (GraphPad Prism).

Identification of phosphorylation sites by tandem mass spectrometry.

In vitro kinase assays were performed using either wild type or D1994A (kinase dead) recombinant LRRK2 plus recombinant substrate, and protein mixture were resolved by SDS-PAGE. The protein bands corresponding to GST-s11, GST-s15 or GST-s27 were excised and subjected to in-gel trypsin digestion. The resulting tryptic peptides were desalted on an in-house trap column (75 μm inner diameter, 2 cm long) packed with C-18 materials (Magic C18AQ, 5 μm, 100 Å) and separated on an in-house analytical column (75 μm inner diameter, 15 cm long) packed with the same packing materials. Separated peptides were analyzed on either an LTQ-Orbitrap Elite ETD mass spectrometer or an LTQ-Orbitrap XL ETD mass spectrometer. The acquired mass spectra data were searched against a human RefSeq protein database using both SEQUEST and MASCOT algorithms. The searching criteria were set as following; maximal 2 missed cleavage allowed; 10 ppm mass tolerance for precursor ions; 0.5 Da

or 0.05 Da mass tolerance for fragment ions for data from an LTQ-Orbitrap XL ETD mass spectrometer or an LTQ-Orbitrap Elite ETD mass spectrometer, respectively; oxidation at methionine, deamidation at asparagine or glutamine, or phosphorylation at serine, threonine, or tyrosine as variable modifications; carbamidomethylation at cysteine as a fixed modification. The probability of phosphorylation sites was calculated by the PhosphoRS algorithm. All tandem mass spectra obtained were manually validated. No phosphorylation sites were detected on substrates incubated with D1994A LRRK2. The sequence coverage for substrates phosphorylated by WT LRRK2 was calculated by dividing the number of amino acid residues encompasses within identified peptides by the total number of amino acid residues in a corresponding protein.

Phospho-s15 polyclonal antibody generation

The s15 phospho-peptide RPGIGA(p)THSSRFIPLKC was conjugated to KLH and injected into rabbits for polyclonal antibody generation. Phospho-s15 antibody was purified from crude sera by passing it over a sulfo-link immobilized peptide column containing s15 phospho-peptide. The eluate was then passed over a sulfo-link immobilized peptide containing non-phosphorylated s15 peptide. The flow-through from this step was subsequently passed over a second phospho-peptide column to obtain purified phospho-antibody.

Enzyme-linked immunosorbent assay for phospho-s15 antibody validation

50 µL of 500 µg/mL s15 oligopeptide or 500 µg/mL T136 Phospho-s15 oligopeptide immunogen were added to separate 96-well plates and incubated on an orbital shaker

overnight at 4°C. All subsequent incubation and detection steps were performed at room temperature. Plates were washed twice in PBS and blocked in a 5% non-fat milk solution in PBS on a shaker for 90 minutes. The plates were washed twice in PBS (5 minutes per wash). T136 Phospho-s15 antibody dilutions in TBS-T with 2.5% non-fat milk were added and incubated for 1 h on a shaker. The plates were washed three times in TBS-T (5 minutes per wash) and anti-rabbit secondary antibody dilutions in TBS-T with 2.5% non-fat milk were added. Secondary antibody was incubated for 1h on a shaker and plates were washed three times in TBS-T (15 minutes per wash). 100 µL of 3,3,5,5-tetramethylbenzidine (TMB) was added to each well. OD (650 nm) was read after 5 minutes incubation.

Dot blot for phospho-s15 antibody validation

Using gel-loading tips, 10 ng of T136 Phospho-s15 oligopeptide immunogen or non-phosphorylated s15 oligopeptide were spotted on pieces of nitrocellulose membrane**.** Spots were allowed to dry and the membranes were cut into strips, marked for orientation. All subsequent incubation and detection steps were carried out at room temperature. Membrane strips were blocked in 5% milk in TBS-T for 30 minutes on a shaker, washed in TBS-T, then incubated in T136 Phospho-s15 antibody at the dilutions indicated for 1h. Membranes were washed three times in TBS-T (5 minutes per wash) on a shaker**.** HCL-conjugated anti-rabbit antibody (diluted 1:1000 in 2.5% milk/TBST) was added and incubated on a shaker for 1 h**.** Membranes were washed three times in TBS-T (15 minutes per wash) on a shaker and antibody detection was performed with enhanced chemiluminescent substrate.

LRRK2 toxicity assays

Rat neurons: Neuronal toxicity was assessed using previously described methods (Lee et al., 2010; Li et al., 2010; Ramsden et al., 2011; Xiong et al., 2010). Primary cortical neuronal cultures were prepared from gestational day 15 fetal rats as previously described. The cortex was dissected, incubated for 15 minutes in 0.027% trypsin, and then transferred to modified Eagle's medium (MEM)/10% horse serum/10% fetal bovine serum/2 mM glutamine followed by trituration. Dissociated cells were plated at a density of 3-4 x 10^5 cells per well in polyornithine-coated plates. After 4 days, the cells were treated with 10 µg of 5-fluoro-2'-deoxyuridine to prevent proliferation of non-neuronal cells. Cells were maintained in MEM/5% horse serum/2 mM glutamine in an 8% CO2 incubator. The medium was changed twice weekly. At DIV 10-12, neurons were switched to Opti-MEM reduced serum medium and transfected with plasmid DNA. Myc LRRK2 (or vector), s15/s11 (or vector) and GFP for tracing neurites at a 10:10:1 ratio were mixed with Lipofectamine 2000 at a 1:3 ratio in Opti-MEM. 4 h after transfection, the medium was replaced with original conditioned medium containing serum. 48 h after transfection, neurons were fixed, permeabilized and immunostained. The vast majority of GFP-positive neurons (~90%) also co-labeled for overexpressed LRRK2 and s15/s11 indicating that the effects of LRRK2 and s15/s11 could be assessed in these neurons, as previously described (Xiong et al., 2010). Neurons were subject to TUNEL and DAPI staining following manufacturer’s protocols and visualized using a Zeiss Axiocam fluorescent microscope with Axiovision 6.0 software. Viable neurons were defined as having at least one smooth extension (neurite) twice the length of the cell body. The percentage of GFP-positive injured neurons in each experimental group relative to all

GFP-positive neurons was calculated. The percentage of GFP-positive neurons exhibiting TUNEL-positive nuclei was also determined. At least 100 neurons were counted per group per independent experiment.

Human neurons: Mature human cortical and dopamine neurons were derived from the H1 embryonic stem cell line using methods described elsewhere (Kriks et al., 2011; Pasca et al., 2011; Yahata et al., 2011) and validated by immunostaining. Human cortical neurons derived from embryonic stem cells by targeted differentiation for 60 d were immunopositive for the neuronal marker MAP2 and synaptic marker synaptophysin. Neurons were immunopositive for cortical layer-specific markers (TBR1 (layers I, V and VI), BRN2 (layers II-IV), SATB2 (layers II-IV, V), and CTIP2 (layer V and VI)). Midbrain dopamine neurons were identified by co-labeling of tyrosine hydroxylase (TH) and the midbrain marker FOXA2 as well as the neuronal marker TUJ1 at day 32 of differentiation. LRRK2 toxicity was assessed in human cortical or dopamine neurons at these time points as described for rat cortical neurons. The use of viral vectors such as the HSV amplicon for gene overexpression was precluded by the known induction of interferon response caused by these vectors, which may significantly affect translation via protein kinase R activation (Shayakhmetov et al., 2010; Suzuki et al., 2007, 2008). For human dopamine neurons, neuronal injury and TUNEL phenotypes were assessed on TH-positive neurons.

Bicistronic reporter assay

A bicistronic reporter (pCMV-BICEP 4, Sigma) which expresses a single transcript with two eGFP open reading frames separated by a CMV IRES, was used to determine the relative effects of LRRK2, s15, s15 knock-down, hAgo2 and dicer on cap-dependent and cap-independent translation via expression of ORF1 (FLAG-eGFP) and ORF2 (c-Myc-eGFP), respectively.

SH-SY5Y neuroblastoma cells: This bicistronic vector was co-transfected into SH-SY5Y cells with LRRK2 and N-terminal tagged V5-s15 variants, 4E-BP or hAgo2 at a ratio of 1:4:4 using X-tremeGENE HP transfection reagent. 36 h after transfection, cells were harvested in chilled PBS, and lysed in extraction buffer (1% NP-40, 50 mM Tris-HCl, 150 mM NaCl, 5 mM EGTA, protease inhibitor cocktail). Equal protein amounts were resolved by SDS-PAGE. Following transfer, membranes were probed with antibodies to detect FLAG, myc, V5, LRRK2 and actin. Relative amounts of eGFP mRNA were determined by reverse transcriptase qPCR using SYBR green dye and the $\Delta\Delta C_t$ method, with the geometric mean of GAPDH, β-actin, α-tubulin and β-2-microglobulin transcripts used as a loading control. For dicer knock-down, 150 nM dicer smart-pool siRNAs were transfected into cells at low confluency, resulting in 80-90% dicer silencing by 48h and concomitant reduction in miRNA levels at this time point (not shown). 48h after initial transfection, a second transfection consisting of bicistronic reporter with or without LRRK2 was performed.

Human cortical neurons: Neurons were transfected with bicistronic vector in addition to LRRK2 and/or s15 variants using Lipofectamine 2000 in Opti-MEM medium. After 4 h,

the medium with transfection complex was replaced with original conditioned medium. 36 h following transfection, neurons were fixed, permeabilized and subject to immunocytochemistry with antibodies to detect eGFP, LRRK2, MAP2, as well as assaying for TUNEL positive cells. The percentage of GFP-positive cells in each treatment group was determined using a cell counting tool in ImageJ on at least 500 cells per group for each independent experiment. A translation-linked neuronal injury index, which describes the amount of neurons exhibiting reporter translation and neurite shortening was derived as follows: % neuronal injury x % reporter-positive neurons x 100%. A translation-linked cell death index was similarly derived as follows: % TUNEL-positive nuclei x % reporter-positive neurons x 100%. LRRK2 toxicity was assessed in reporter (eGFP)-positive, MAP2-positive neurons and reporter-negative, MAP2-positive neurons using the methods described above.

Phospho-s15 in human cortical neurons

Phosphorylation of endogenous s15 at T136 following LRRK2 overexpression was measured in human cortical neurons (derived and characterized as described above). Cultures were transduced with an HSV amplicon vector previously described (Lee et al., 2010) containing untagged LRRK2, D1994A LRRK2, G2019S LRRK2 or GFP. 48 h after transduction, neurons were harvested by gentle scraping in chilled PBS, briefly centrifuged and resuspended in lysis buffer (1% NP-40, 50 mM Tris-HCl, 150 mM NaCl, 5 mM EGTA, 20 mM protease inhibitor cocktail, β-glycerophosphate, 10 mM sodium fluoride, 1% serine/threonine phosphatase inhibitor cocktail (Sigma)). Samples were incubated on ice for 30 minutes, centrifuged at 18, 000 x g, and supernatants were

subject to SDS-PAGE followed by immunoblotting for endogenous T136 Phospho-s15, total s15, LRRK2 and actin.

LRRK2 and s15 colocalization in human cortical neurons or *Drosophila* S2 cells

Human cortical neurons derived as described above or Drosophila S2 cells were fixed in 4% paraformaldehyde, washed three times in PBS, blocked in 10% donkey serum/0.3% triton-X-100 and immunostained for endogenous s15 (Abcam or Sigma) and LRRK2 (NeuroMab) or endogenous dLRRK (gift from Bingwei Lu) overnight at 4°C followed by three 5 minute washes in PBS then incubation in alexa-fluor 488 and alexa-fluor 568. Neurons were visualized using confocal microscopy. Assessment of G2019S LRRK2 colocalization was carried out as above, 2d after LRRK2 transfection using Lipofectamine 2000 as before.

LRRK2 and s15 co-immunoprecipitation

Protein G-antibody complexes (Dynabead protein G) were prepared and incubated overnight at 4°C. The following day, HEK293FT cells were lysed in cell lysis buffer (10mL Tris-HCl pH 7.5, 150mL NaCl, 5mM EGTA, 1% Nonidet P-40 (vv) and Complete Protease Inhibitor Mixture). Co-immunoprecipitation was performed by incubating lysates with the respective Dynabead-protein G-antibody complexes overnight at 4ºC, either LRRK2 (Cell Signaling) or s15 (Sigma). The immunocomplexes were washed with wash buffer (PBS and Complete Protease Inhibitor Mixture) for four times and protein was eluted by adding sample loading buffer and heating to 70°C for 10 min.

Drosophila stocks and husbandry

All flies were reared and aged at 25°C/60% relative humidity under a 12 h light-dark cycle on standard cornmeal medium. Human s15 and T136A s15 constructs were generated by subcloning full-length cDNA into pUAST between EcoR1 and Xba1 restriction sites. After sequence verification, constructs were microinjected into w^{1118} fly embryos. Transgenic *UAS-s15* and *UAS-T136A s15* expression were confirmed by western blot on fly heads following expression driven via *daughterless-Gal4* (Fig. S5A). Transgenic human LRRK2 (WT and G2019S) lines previously characterized (Liu et al., 2008) were generously provided by Wanli Smith. All other lines were obtained from the Bloomington *Drosophila* stock center.

Phospho-s15 in *Drosophila* or human post-mortem brain

Whole Drosophila heads from control or LRRK2 transgenic flies were lysed in extraction buffer and ribosomal fractions were isolated essentially as described before (Belin et al., 2010) with the addition of phosphatase inhibitors to the extraction buffer. Ribosomal fractions were washed twice in 1 ml of chilled water before resuspension in buffer C. Total protein concentrations were determined using the Lowry assay. 40 µg of total protein for lysates and ribosomal fractions were loaded onto polyacrylamide gels, separated by SDS-PAGE and immunoblotted. For human brain samples, whole lysates were run on separate gels due to the limited number of lanes per mini-gel.

Drosophila dopamine neuron immunohistochemistry

Brains were harvested, fixed and permeabilized at 7 weeks of age and immunohistochemistry for tyrosine hydroxylase expressing neurons was performed following methods previously described (Wu and Luo, 2006). Confocal z-stacks were acquired at 1 µm slice intervals and projection images through the anterior portion of the brain for the PAL (protocerebral anterior lateral) cluster and posterior brain for the PPM1/2 (protocerebral posterior medial 1/2), PPM3, PPL1 (protocerebral posterior lateral 1) and PPL2 clusters were derived and used for dopamine neuron counts.

Drosophila negative geotaxis

Cohorts of 75 female flies back-crossed to an isogenic w^{1118} background for six generations were collected under brief anesthesia and transferred to fresh food vials to recover. After 24 h, flies were transferred to empty vials, allowed 1 min to rest and then tapped to the bottom of the vial to initiate climbing. The position of each fly was captured in a digital image 4 s after initiation using a fixed camera. A second group of flies collected at the same time were aged for 6 weeks (or as indicated) and tested using the same protocol. Automated image analysis was performed on digital images using the particle analysis tool on Scion Image to derive x-y co-ordinates for each fly thus providing the height climbed, as described before (Gargano et al., 2005). Young and aged flies were tested at the same time of the day.

35S-methionine/cysteine labeling in *Drosophila*

35S-methionine/cysteine (100 µCi/ml) was added to standard food medium during cooling. The following day, flies were transferred to labeled food for 24h, and then

heads were collected on dry ice and homogenized by pestle and mortar in 1% NP-40 extraction buffer on ice. Protein was precipitated by the addition of methanol and heparin (lysate:heparin(100mg/ml):methanol volume ratio of 150:1.5:600), centrifuged at 14,000 x g for 2 minutes, and supernatant was removed and the pellet air dried. Protein pellet was resuspended in 8M urea/150 mM Tris, pH 8.5 and incorporation relative to total protein amount was measured by scintillation counting following assay of protein concentration by BCA assay.

Anisomycin treatment in *Drosophila*

Anisomycin (or DMSO vehicle) was added to standard food medium at a final concentration of 10 µM anisomycin/0.1%DMSO. Flies were transferred to fresh food containing anisomycin/vehicle at 3-4 d intervals and aged for assessment of dopamine neuron viability and negative geotaxis performance, as described above.

mRNA polysome profiling by RT-PCR

Fly heads were homogenized in polysome lysis buffer (10 mM Tris-HCl/150 mM NaCl/5 mM $MgCl_2$/0.5 mM DTT/100 µG cycloheximide/EDTA-free protease inhibitor cocktail/40U/ml Superase-in) and following clearing of the homogenate by centrifugation at 2,000 x g for 10 minutes, 1% NP-40 was added to the supernatant and incubated on ice for 10 minutes. The lysate was cleared by centrifugation at 16,000 x g for 10 mins at 4°C, lysate was then layered onto a 10-60% sucrose gradient, centrifuged in a SW-41Ti rotor at 40,000 rpm for 2 hours at 4°C, and sampled using a Biocomp gradient station connected to a Gilson fraction collector with constant monitoring of optical density at

254 nm. 1 ml fractions were collected and spiked with 20 ng of polyA synthetic luciferase RNA to control for variations in downstream processing as previously described (Thoreen et al., 2012). Total RNA was extracted from each fraction using Trizol LS (Life Technologies) and precipitated with isopropanol following the manufacturer's protocol. cDNA was derived using Superscript III first-strand kit for RT-PCR using random hexamer primers and following the manufacturer's protocol. Transcript levels were measured by quantitative PCR using SYBR green master mix (Applied Biosystems) and primers for actin 5C, tubulin or luciferase. Actin 5C and tubulin levels in each fraction were normalized to luciferase and the percentage of translated mRNA in each fraction was calculated relative to the total RNA in all monosome and polysome fractions combined.

Assessment of ribosomal runoff

SH-SY5Y cells were transfected with LRRK2 and the following day, passaged to a new culture vessel at ~40% confluency to allow exponential growth. 24h after passaging, cells were treated with harringtonine (2 μg/ml) to freeze initiating ribosomes and allow runoff of elongating ribosomes. Total ribosomal translocation was blocked by adding cycloheximide (100 μg/ml) at fixed time intervals following harringtonine, and polysome profiles were generated by sedimentation of cell lysates made using polysome lysis buffer on 10-60% sucrose gradients. In a parallel experiment, transfected cells were pulse labeled with ^{35}S-methionine/cysteine (50 μCi/well) then immediately treated with harringtonine and cycloheximide together or harringtonine followed by cycloheximide at fixed time intervals. Cells were lysed and increase in ^{35}S-methionine/cysteine

incorporation was measured and compared between groups as an indicator of relative ribosomal elongation rates.

LRRK2 subcellular fraction studies

HEK293 cells were fractionated using a centrifugation protocol described elsewhere (Belin et al., 2010) to derive nuclear, mitochondrial and ribosomal fractions. Protein concentrations for lysates and fractions were determined using the Lowry assay. 40 µg of total protein for lysates and fractions were resolved by SDS-PAGE. Membranes were blotted for LRRK2 and nuclear, mitochondrial and ribosomal fraction markers.

Real time PCR primer sequences

d.m. actin 5C (fwd 5'-GTGAAATCGTCCGTGACATC-3'; rev 5'-GGCAGCTCGTAGGACTTCTC-3'). *d.m. α-tubulin* (fwd 5'-CACTTCCAATAAAAACTCAATATGCGTGA; rev 5'-ACAGTGGGTTCCAGATCCAC-3'). *luciferase* (fwd 5'-TGGAGAGCAACTGCATAAGG-3'; rev 5'-CGTTTCATAGCTTCTGCCAA-3'). *eGFP* (fwd 5'-ACGTAAACGGCCACAAGTTC-3'; rev 5'-AAGTCGTGCTGCTTCATGTG-3'). *h.s. GAPDH* (fwd 5'-AAACCCATCACCATCTTCCAG-3'; rev 5'-AGGGGCCATCCACAGTCTTCT-3'). *h.s. α-tubulin* (fwd 5'-CGCCCAACCTACACTAACCT-3'; rev 5'-ATTCAGGGCTCCATCAAATC-3'). *h.s. β-2-microglobulin* (fwd 5'-GACTTTGTCACAGCCCAAGA-3'; rev 5'-CAAGCAAGCAGAATTTGGAA-3'). *h.s. β-actin* (fwd 5'- AGCCTCGCCTTTGCCGA-3'; rev 5'-GCGCGGCGATATCATCATC-3').

References:

Gargano, J.W., Martin, I., Bhandari, P., and Grotewiel, M.S. (2005). Rapid iterative negative geotaxis (RING): a new method for assessing age-related locomotor decline in Drosophila. Exp Gerontol *40*, 386-395.

Kriks, S., Shim, J.W., Piao, J., Ganat, Y.M., Wakeman, D.R., Xie, Z., Carrillo-Reid, L., Auyeung, G., Antonacci, C., Buch, A.*, et al.* (2011). Dopamine neurons derived from human ES cells efficiently engraft in animal models of Parkinson's disease. Nature *480*, 547-551.

Pasca, S.P., Portmann, T., Voineagu, I., Yazawa, M., Shcheglovitov, A., Pasca, A.M., Cord, B., Palmer, T.D., Chikahisa, S., Nishino, S.*, et al.* (2011). Using iPSC-derived neurons to uncover cellular phenotypes associated with Timothy syndrome. Nat Med *17*, 1657-1662.

Shayakhmetov, D.M., Di Paolo, N.C., and Mossman, K.L. (2010). Recognition of virus infection and innate host responses to viral gene therapy vectors. Mol Ther *18*, 1422-1429.

Suzuki, M., Chiocca, E.A., and Saeki, Y. (2007). Early STAT1 activation after systemic delivery of HSV amplicon vectors suppresses transcription of the vector-encoded transgene. Mol Ther *15*, 2017-2026.

Suzuki, M., Chiocca, E.A., and Saeki, Y. (2008). Stable transgene expression from HSV amplicon vectors in the brain: potential involvement of immunoregulatory signals. Mol Ther *16*, 1727-1736.

Wu, J.S., and Luo, L. (2006). A protocol for dissecting Drosophila melanogaster brains for live imaging or immunostaining. Nat Protoc *1*, 2110-2115.

Yahata, N., Asai, M., Kitaoka, S., Takahashi, K., Asaka, I., Hioki, H., Kaneko, T., Maruyama, K., Saido, T.C., Nakahata, T.*, et al.* (2011). Anti-Abeta drug screening platform using human iPS cell-derived neurons for the treatment of Alzheimer's disease. PLoS One *6*, e25788.

Supplemental Figure 1

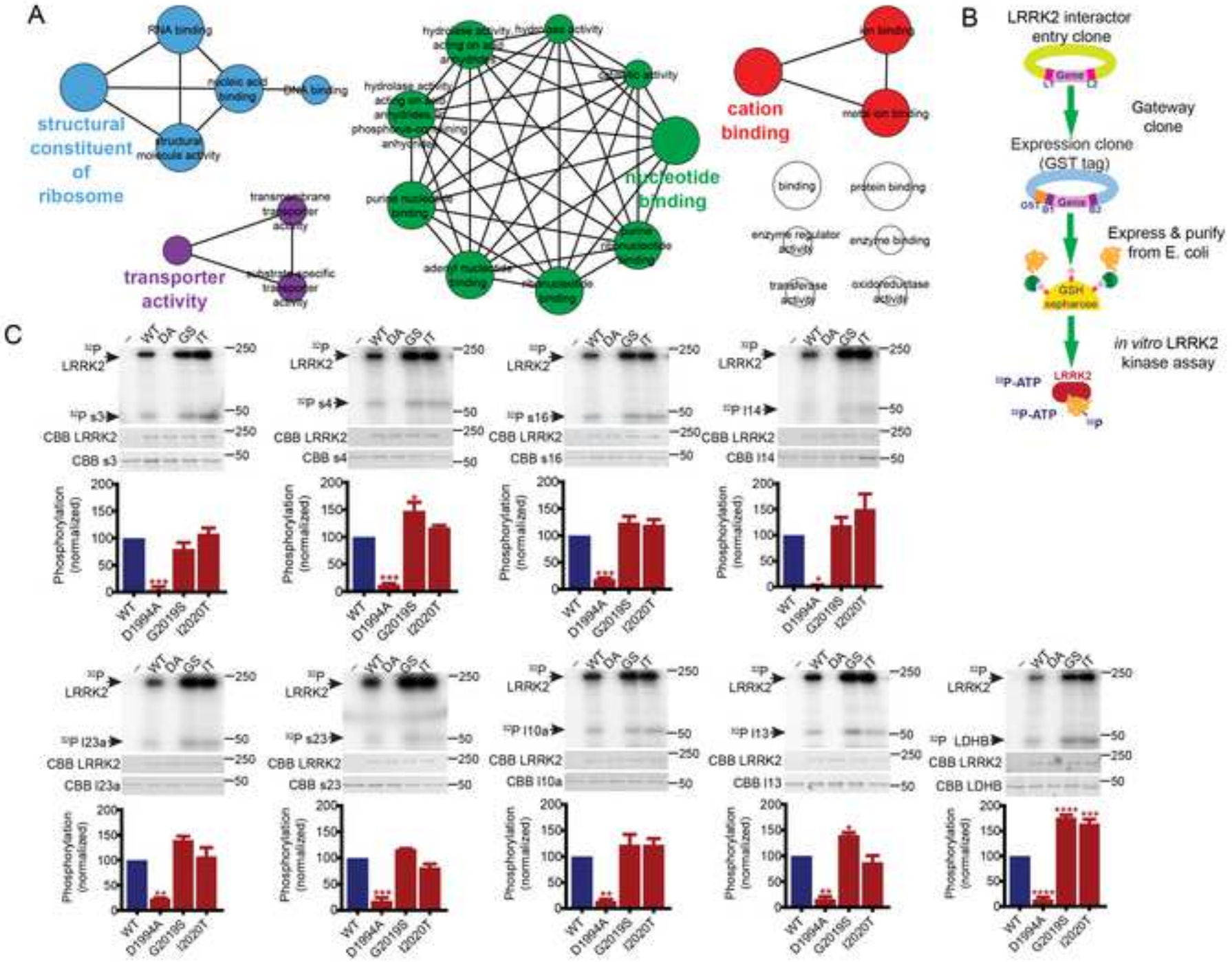

Supplemental Figure 2

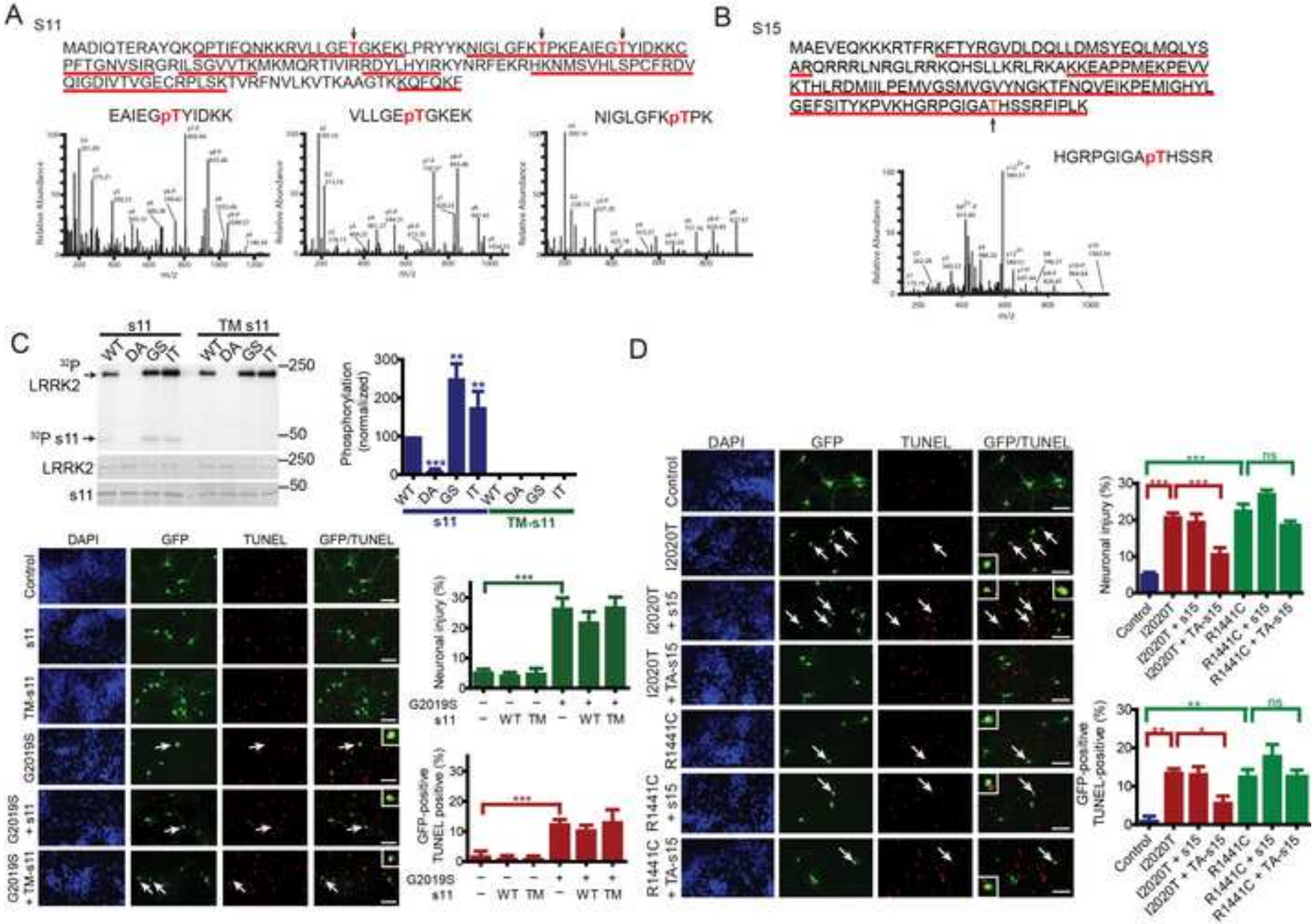

Supplemental Figure 3

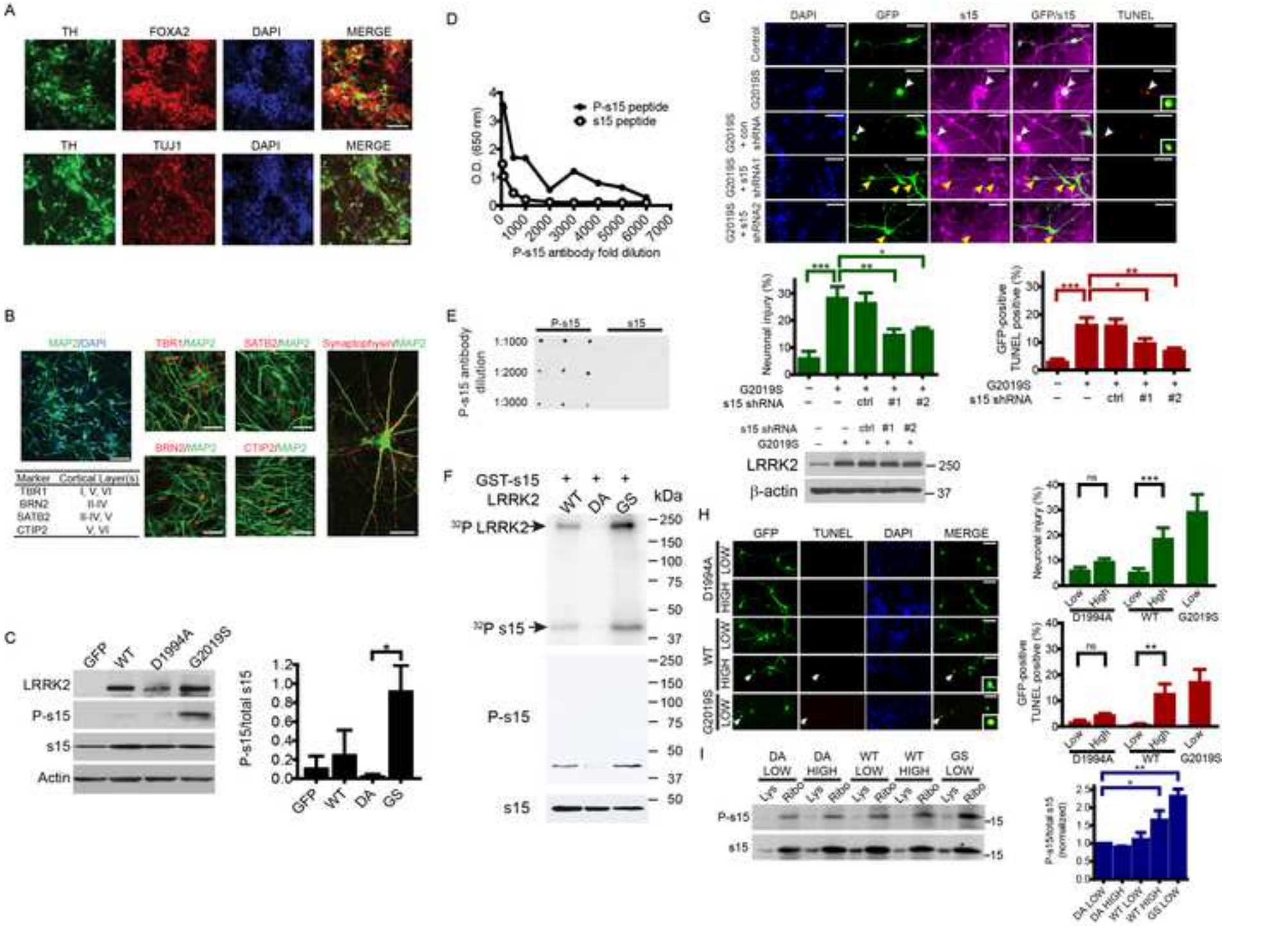

Supplemental Figure 4

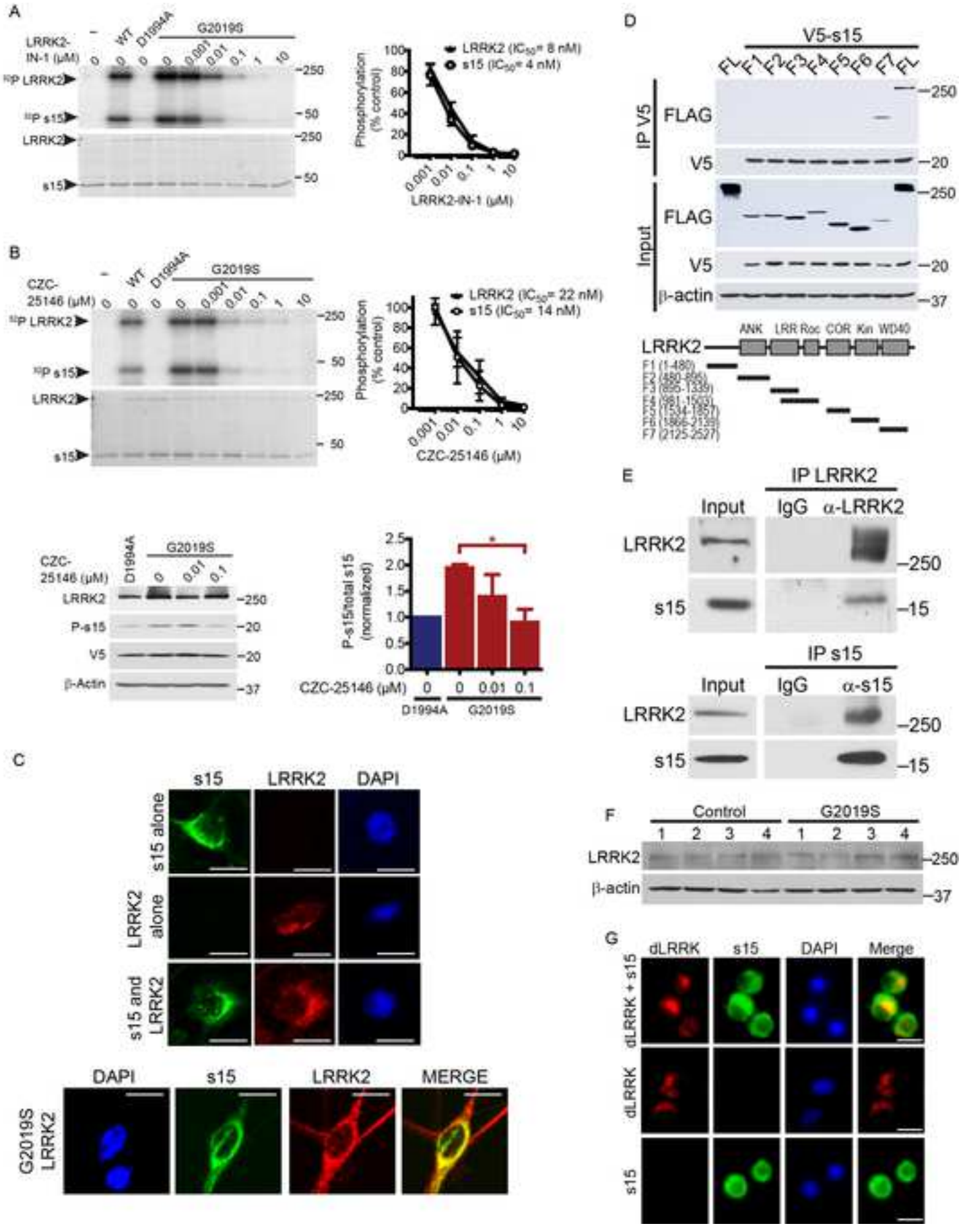

Supplemental Figure 5

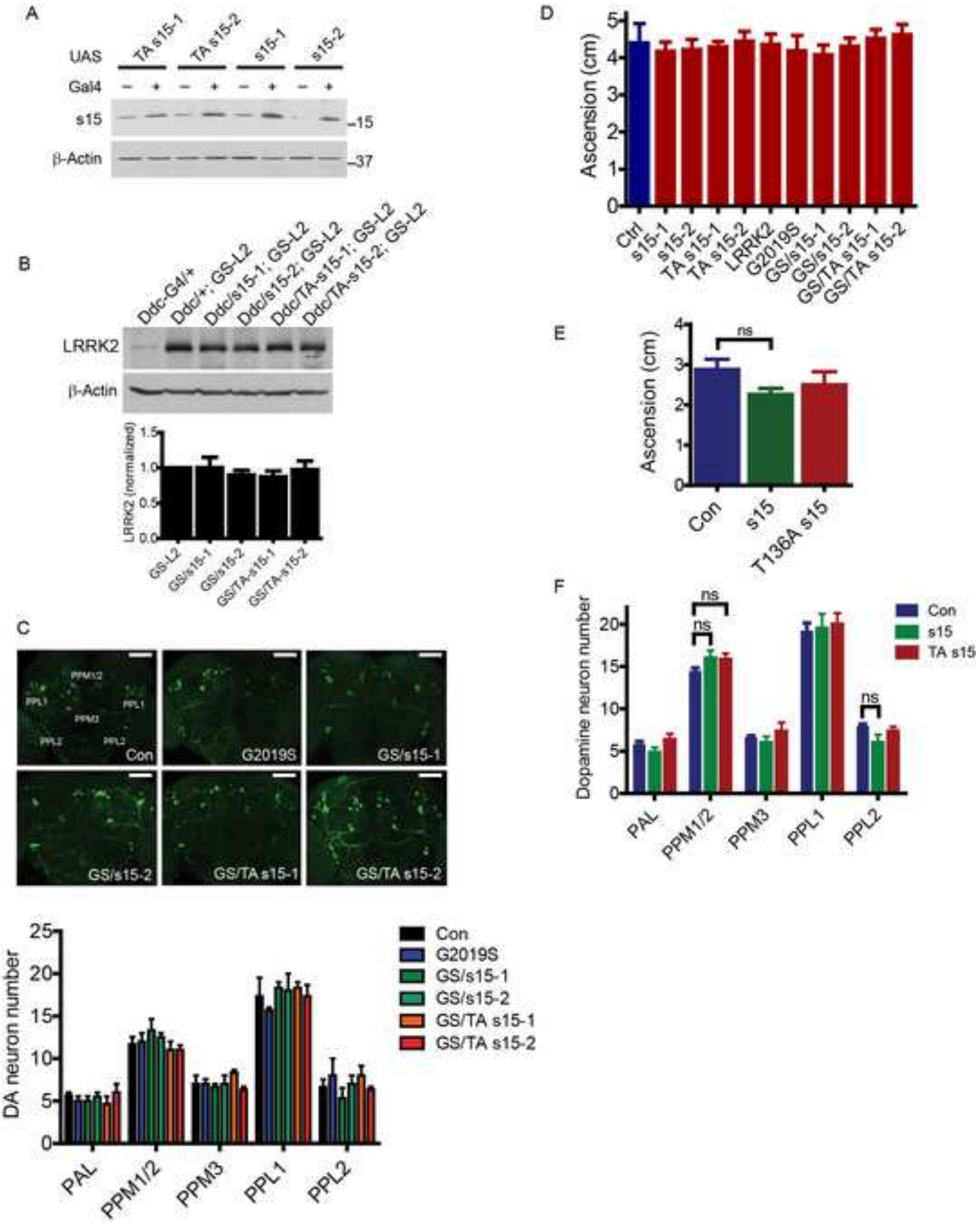

Supplemental Figure 6

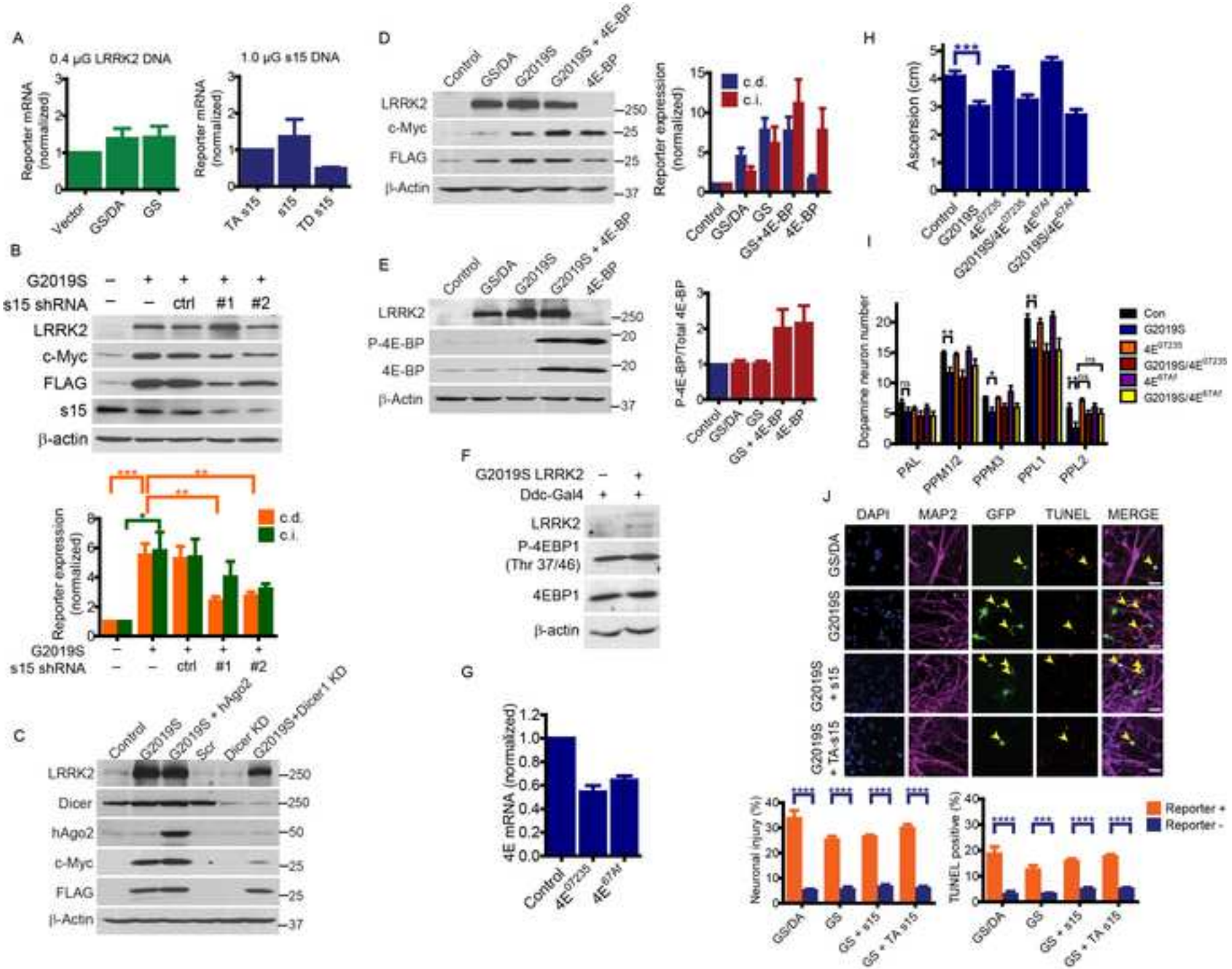

Supplemental Figure 7